International Journal of Computing and Digital Systems
ISSN (2210-142X)
Int. J. Com. Dig. Sys. #, No.# (Mon-20..)

Elman Recurrent Neural Network-based Digital Electrical Measuring Unit for Transmitter Antenna Underground Imaging System

Jonah Jahara Baun[1,3,*], Adrian Genevie Janairo[1,3], Ronnie Concepcion II[2,3], Kate Francisco[2,3], Mike Louie Enriquez[2,3], R-Jay Relano[2,3], Edwin Sybingco[1], Argel Bandala[1,3], Ryan Rhay Vicerra[2,3]

[1]Department of Electronics and Computer Engineering, De La Salle University, Manila, Philippines
[2]Department of Manufacturing Engineering and Management, De La Salle University, Manila, Philippines
[3]Center for Engineering and Sustainability Development Research, De La Salle University, Manila, Philippines

E-mail address: jonah_baun@dlsu.edu.ph, adrian_janairo@dlsu.edu.ph; ronnie.concepcion@dlsu.edu.ph; kate_g_francisco@dlsu.edu.ph; mike_louie_enriquez@dlsu.edu.ph; r-jay_relano@dlsu.edu.ph; edwin.sybingco@dlsu.edu.ph; argel.bandala@dlsu.edu.ph; ryan.vicerra@dlsu.edu.ph

Received ## Mon. 20##, Revised ## Mon. 20##, Accepted ## Mon. 20##, Published ## Mon. 20##

Abstract: Underground imaging equipment is a non-destructive technology for scanning of subsurface which is composed of transmitter and receiver antennae used for measuring underground resistivity. Real-time monitoring of output electrical parameters of the transmitted signals is required since these are significant in the computation of subsurface resistivity. This study aims to develop a digital measuring circuit for monitoring of transmitter antenna output current and voltage and to simulate prediction models that can be implemented in the circuit. Three neural network models-Elman recurrent neural network (ERNN), long short-term memory (LSTM), and gated recurrent unit (GRU) were explored to make prediction models for current and voltage of the transmitter circuit. The performance of the prediction models was assessed using mean squared error (MSE), which is reduced to its absolute lowest value. The result shows that the best-trained models both for current and voltage prediction are the ERNN models with configurations of 900-600-500 hidden neurons network with training MSE of 9.82×10^{-9} and the configured 1300-1000-900 hidden neurons with training MSE of 0.465, respectively. With the help of the prediction models, it would be possible to measure current and voltage output more precisely while avoiding the need for separate and bulky measuring devices.

Keywords: transmitter antenna, digital measuring circuit, recurrent neural network, long short-term memory, gated recurrent unit, underground imaging

1. INTRODUCTION

Underground utility demand in the Philippines was projected to have an increasing trend as there is a constantly growing population rate from 1960 to 2021 with 26.27 million to 111.05 million people, respectively [1]. Increasing population and industrial expansion both contribute to the establishment of various underground service utility lines such as pipes, water lines, electricity, and drainage [2]. With that, it introduces the exploration of utility and object detection through underground imaging technology to properly handle the web of utility lines. This has been a well-known strategy since it has a non-destructive approach to detecting underground utilities, reducing the pre-construction process's unpleasant effect [2]. A capacitive resistivity underground imaging system is composed of a configured transmitter and receiver antennas that are capacitively coupled in the ground [3-4] to measure the potential difference in resistivity readings [5]. The transmitter emits low-frequency electromagnetic waves into the ground and the multi-receiver systems will detect the reflected signals generated by a conductive anomaly [6]. Thus, this concept conveys that penetration, resolution capabilities, and

E-mail: jonah_baun@dlsu.edu.ph

frequency selection are incorporated into a well-configured antenna design.

Numerous designs of transmitter antennae appropriate for subsurface imaging have been developed over the years [7-8]. One study utilized a circular patch antenna with a half-defected ground plane operating from 500 MHz to 2 GHz that is suitable for GPR application of buried object detection [9]. Another design utilized two Marx transistor-based pulse generators, a balun, and a Vivaldi antenna to make a high-power Gaussian monopulse ultrawideband transmitter for buried object detection [10]. Moreover, a transmitter unit which is a transverse electromagnetic flared (TEM) horn antenna with a pulse shaping circuit consisting of a crystal oscillator with an oscillation frequency of 10 MHz and an amplitude in the range of ±1 V has been developed for imaging of water pipelines [11]. Hence, in utilizing transmitter antenna design, one important factor is to have monitoring the current and voltage to verify the parameters of output signals that are essential for the calculation of the subsurface resistivity, and this can be done through a measuring device such as the digital multimeter.

Digital multimeter (DMM) has various measuring capabilities such as Alternating Current (AC) /Direct Current (DC) voltage, current, resistance, power, and electric energy [12]. Since it is a functional electronic device, there are advancements employed to it in recent years. In [13], a digital multimeter was incorporated into the use of a dual-slope Analog-to-Digital Converter (ADC) and a designed algorithm that enabled an accurate determination of power and true Root Mean Square (RMS) voltage. Additionally, voltage and current were measured in a stroboscopic technique. Furthermore, one study has developed an automatic calibration system for a digital multimeter [14] while in [15] additional function was added to the DMM that can observe and record data in real time. Hence, through these innovations, DMM can have more reliable performance and high accuracy in measurement. However, it is crucial to further guarantee that the accurate and scientific process of current and voltage measurements is observed as this is functional in the electrical and electronic industry.

There are many accounts that deep learning was applied in the generation of prediction models for voltage and current measuring models. In the study of [16], researchers compared neural network prediction models, support vector machine (SVM) for regression, and equation discovery for predicting the next voltage values without performing measurements. Another prediction modeling was employed through a convolutional neural network to recognize and classify welding current in order to construct an ERT imaging trailer and detect defects [17]. Additionally, a deep recurrent neural network was employed in forecasting electricity usage in medium to long-term periods [18]. Interestingly, researchers are exploring other neural network models for optimization and prediction applications such as recurrent neural networks which are appropriate for time-series data processing [19] and sequence analysis [20]. Thus, the most known recurrent architectures are the long short-term memory (LSTM) [21] that enables each recurrent unit to control dependencies of different time scales [22]; and the gated recurrent unit (GCU) [23] which is commonly applied in sequential and temporal data [24].

In digital multimeters, it is important to consider the accuracy of electrical parameter readings to reduce and avoid deviation from their actual value. Additionally, there is a need for real-time checking of the generated current and voltage by a single-pair antenna transmitter subsystem for underground imaging to verify the parameters of output signals in comparison to received signals of the receiver subsystem which is essential in calculating the underground's resistivity.

With that, the study focuses on the development of a digital meter with improved accuracy of displayed electrical outputs suitable for underground imaging applications. Three neural network models-Elman recurrent neural network (ERNN), long short-term memory (LSTM), and gated recurrent unit (GRU) were explored to create time-series prediction models for current and voltage outputs of the transmitter circuit. To determine whether the developed measuring device's performance is acceptable, mean squared error (MSE) was reduced to its absolute minimum using the different neural network models. Thus, this allowed simultaneous data acquisition through a single connection from the transmitter of a single-pair antenna system for underground imaging. These prediction models contributed to providing a more accurate output reading of current and voltage which avoids the utilization of a separate, bulky, and multiple connection measuring device.

2. MATERIALS AND METHOD

This research involves five major steps in the prediction and optimization of a current-voltage digital meter for monitoring of transmitter subsystem for underground imaging (Fig. 1). It starts with the construction of the transmitter antenna circuit with current-voltage measuring circuit, then simulation of the circuitry for the collection of measured current and voltage data based on measured DC input voltage (V_{dc}) and set operating frequency (f_o), followed by the development of the different neural network models specifically ERNN, LSTM, and GRU to predict the current and voltage. After that, training, validation, and testing of neural network models were conducted, and lastly, the selection of the best neural network model with the lowest MSE and comparison of its results with the measured values.

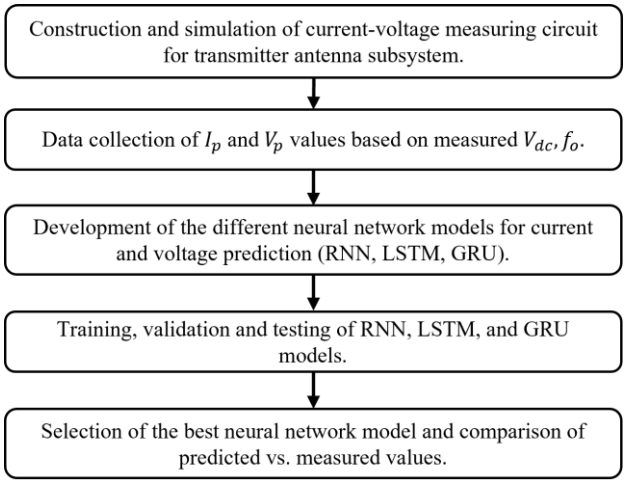

Figure 1. Step-by-step process of the prediction and optimization of current-voltage digital meter for monitoring of transmitter subsystem for underground imaging using recurrent neural network, long short-term memory, and gated recurrent unit.

A. Construction of Measuring Circuit and Digital Signal Processing for Arduino Data Collection

This study's transmitter circuit to be monitored was designed to operate at frequencies from 3.5 KHz to 18.5 KHz. Its signal generator made the transmitter capable of having outputs of two sine, triangular or rectangular waveforms. The range of output voltage is from 500 V_{pk} to 1500 V_{pk} with a minimum power of 2 W and a maximum power of 20 W. To achieve a 10 W output power, its corresponding output voltage must be 10 W. While at maximum power output, the maximum current is close to 15 mA.

Electrical parameters required for proper measurement and analysis of the resistivity of underground imaging using the capacitive resistivity technique are the transmitter's output current and voltage, and the receiver's reading voltage and phase difference. These electrical measurements are essential for the computation of the ground equivalent resistance using Ohm's Law [25]. The digital multimeter (Fig. 2), designed in this study, focused on acquiring measurements from the transmitter subsystem, therefore with readings of the output current and voltage. The process includes analog signal processing from the output of the transmitter and digital signal processing from the output signal of the measuring circuit to the Arduino. The main purpose of the transmitter measuring circuit is to extract a signal from the output of the transmitter and convert it into signals that are within the input threshold of Arduino or any microcontroller, usually 0-3 V. The designed measuring circuit using Proteus simulation software is composed of a 500 μΩ shunt resistor for current extraction from the output of the transmitter, represented by a current source for isolated simulation. Its corresponding voltage at the shunt resistor is amplified with a gain of around 322641 using a 3-stage cascaded amplifier. The amplified AC signal is converted to a DC signal using a peak detector circuit which is an input in the A1 ADC pin of the Arduino. A parallel connection was made from the output of the cascaded amplifier connected to a comparator for pulse generation that has an output of 0 to 2.5 $V_{pk\text{-}pk}$. This pulse signal is the other input to Arduino using an A0 ADC pin.

The DC voltage at the A1 10-bit ADC pin is measured and needed to be converted to its equivalent transmitter peak current, thus simulations were performed to compile relationships between the input current and the measured DC voltage.

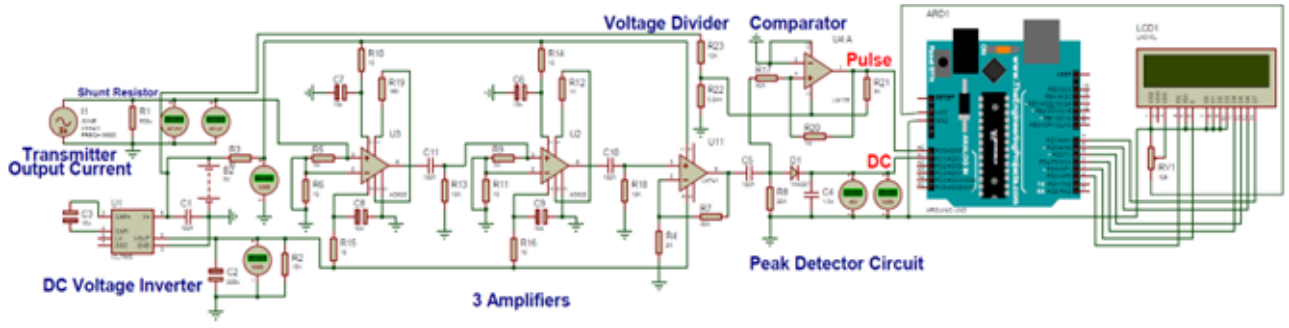

Figure 2. Transmitter Monitoring System (Digital Multimeter) designed using Proteus Simulation Software. Contains the Measuring Circuit, Arduino Uno, and an LCD Display.

To consider the effect of the coupling and parasitic capacitances acting as filters varying the frequency response of the measuring circuit, different input frequencies were also listed in the dataset representing the transmitter output current as a function of the measured DC signal and operating frequency that is measured from the pulses at the input of A0 ADC pin. The resulting 139-row dataset contains operating frequencies ranging from 3.178 KHz to 18.5 KHz, 0.487 V_{DC} to 2.5 V_{DC}, and a current of 4 mA to 15 mA. With the established dataset for model training for current prediction, the next step is to acquire the relation of the transmitter output peak voltage to be defined by the predicted current. Simulations were performed with the transmitter circuit, and it was observed that the relationship between the output voltage and current was not perfectly linear, therefore there is a need to create another dataset for peak voltage prediction to lessen the error compared to an MSE of 62 from multiplying the current with the average computed load of 102.54 Ω. The second dataset is composed of 419 rows of relationships of the transmitter peak currents and voltages ranging from 4 mA to 15 mA and 411 V_{pk} to 1485 V_{pk}, respectively.

B. *Recurrent Neural Network*

Recurrent neural networks (RNNs) are an advanced deep learning prediction and classification method that are particularly well suited to handling time-series data and other sequential data [26] that performs well and most sophisticated method for machine learning, and natural language processing [19]. Typically, an RNN's hidden state h_t dynamics given an input sequence $x = x_1, x_2, \ldots, x_t$ may be expressed as:

$$h_t = \begin{cases} 0 & if\,(t = 0) \\ \emptyset(h_{t-1}, x_t), & otherwise \end{cases} \quad (1)$$

where $\emptyset$ is a non-linear function while the updated recurrent hidden state is stated as follows:

$$h_t = \sigma(Wx_t + Uh_{t-1}) \quad (2)$$

where σ is a hyperbolic tangent function, W is the input neuron weight, and U is the recurrent neuron weight. Thus, the output Z at time t is calculated as:

$$Z_t = (Wh_y \cdot h_t) \quad (3)$$

where Wh_y is the corresponding weight at the output layer.

In this study, the prediction of the current level has been performed specifically using the Elman recurrent neural network (ERNN) architecture presented in Fig. 3 whereas there are two inputs (DC input voltage and operating frequency), three hidden layers, and one expected output for predicted current.

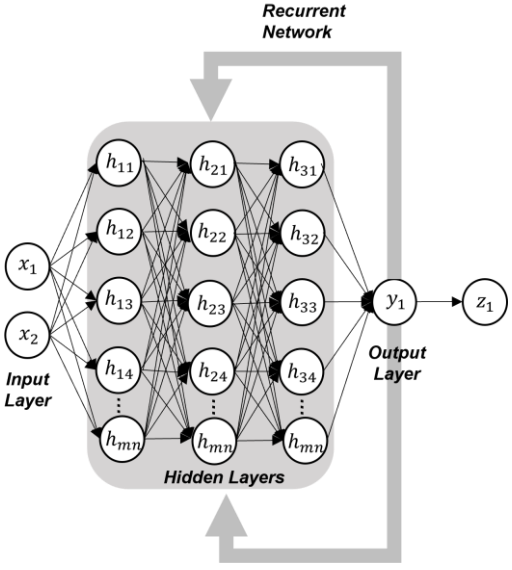

Figure 3. The designed Elman recurrent neural network architecture for current signal prediction.

C. *Long Short-Term Memory*

The LSTM model was created to address the inadequacies of RNNs, for the purpose of capturing long-term information and improving performance on long sequence data [27], To overcome the problems of disappearing gradients and gradient expansion, LSTM introduces input gates and forget gates [28].

The LSTM layers are comprised mainly of four gates that manipulate the cell-state data. The first is referred to as the "forget gate," which recognizes and omits data that is optional and not necessary. Furthermore, the sigmoid function also defines which from the old output can be eliminated. It is followed by the input gate, where the sigmoid function defines whether the data will be written or ignored. The next layer is the candidate gate with the

E-mail: jonah_baun@dlsu.edu.ph

tanh functions that weigh the importance of the data and control what to write in the cell state. Finally, the output gate specifies what data should be sent as the output concealed state h_t through filtering with the sigmoid function multiplied by the new values created by the tanh layer from the cell state c_t [29]. The cell state is in charge of adding or eliminating previous data based on its relevance and importance in making the forecast [27].

$$i_t = \sigma(x_t U^i + h_{t-1} W^i) \quad (4)$$

$$f_t = \sigma(x_t U^f + h_{t-1} W^f) \quad (5)$$

$$o_t = \sigma(x_t U^o + h_{t-1} W^o) \quad (6)$$

In (4) to (6), i_t, f_t, and o_t represent the input gate, forget gate, and output gate where σ is the sigmoid function, x_t is the input given, U^i, U^f, and U^o represent the weight of the input in the input, forget, and output gates respectively, h_{t-1} holds the data from the preceding terms, while W^i, W^f, and W^o are the weights of the data from the preceding terms in the input, forget, and output gates. Then, the cell state c_t is given to tanh function and multiplied to o_t to get the updated hidden state h_t.

D. Gated Recurrent Unit

The gated recurrent unit is a specific kind of optimized LSTM-based recurrent neural network that keeps the LSTM immunity to the vanishing potential problem. Updating the internal states requires less work since the underlying structure is simpler and easier to train. The reset port decides whether the current state should be coupled with the prior information, while the update port governs how much of the state data from the last instant is maintained in the present condition. GRU requires less memory and is quicker than LSTM. However, when working with datasets that comprise longer sequences, LSTM is accurate to a greater extent [28]. GRU's input and output structures are identical to those found in a standard RNN, while its internal structure is comparable to an LSTM [28]. A typical GRU is composed of reset gate r and update gate z which can be calculated as:

$$r_t = \sigma(x_t W_r + h_{t-1} U_r) \quad (6)$$

$$z_t = \sigma(x_t W_z + h_{t-1} U_z) \quad (7)$$

where σ is the sigmoid function, x_t is the given input, W_r and W_z are the weights in the input of the reset and update gate, respectively, h_{t-1} holds the data of the preceding units while U_r and U_z represent the weights of the preceding units in the reset and update gate, accordingly. Finally, the hidden state h_t is calculated using the hidden state of time $t-1$ and input time series value x_t.

Additionally, the LSTM and GRU architecture for current prediction used in this study is presented in Fig. 4. It represents two inputs (DC input voltage and operating frequency), three hidden layers, a fully connected layer, and one expected output for predicted current.

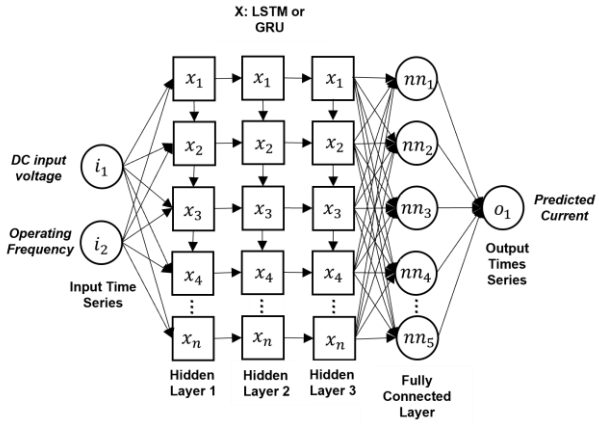

Figure 4. The designed LSTM and GRU network architecture for current signal prediction.

E. Peak Voltage and Peak Current Prediction using ERNN, LSTM, and GRU

The ERNN, LSTM, and GRU were coded and performed using MATLAB Software. The ERNN was modeled using the hyperparameters presented in Table 1 while LSTM and GRU are shown in Table 2. Each of the three neural network models is composed of three hidden layers wherein in hidden layer 1, the simulated number of neurons was set to 500, 700, 900, 1100, and 1300, in hidden layer 2 was 200, 400, 600, 800, 1000, and in hidden layer 3 was 100, 300, 500, 700, 900. The number of training epochs for the three models was set to 500, 1000, 1500, 2000, and 2500.

The logarithmic transfer function 'logsig' has been used as the activation function for each of the three hidden layers in the optimum network architecture in ERNN, linear transfer function 'purelin' has been used in the output layer, while 'trainrp' is used as the network training function by which in accordance with the resilient backpropagation method, it adjusts the weight and bias values.

To update the network learnable parameters in a custom training loop in LSTM and GRU model for current prediction, the stochastic gradient descent with momentum (SGDM) algorithm was applied. On the other hand, for voltage prediction, the adaptive moment estimation optimizer (ADAM) was employed. Lastly, an initial learning rate of 0.01 and a minibatch size of 128 were also used in LSTM and GRU models.

TABLE I. HYPERPARAMETERS FOR CURRENT AND VOLTAGE PREDICTIONS USING ERNN

Hyperparameter	Value
Number of Neurons for Hidden Layer 1	500, 700, 900, 1100, 1300
Number of Neurons for Hidden Layer 2	200, 400, 600, 800, 1000
Number of Neurons for Hidden Layer 3	100, 300, 500, 700, 900
Number of Training Epochs	500, 1000, 1500, 2000, 2500
Activation Function for Hidden Layer 1	Logsig
Activation Function for Hidden Layer 2	Logsig
Activation Function for Hidden Layer 3	Logsig
Output Layer Activation Function	Purelin
Training Function	Trainrp

TABLE II. HYPERPARAMETERS FOR CURRENT AND VOLTAGE PREDICTIONS USING LSTM AND GRU

Hyperparameter	Value
Number of Neurons for Hidden Layer 1	500, 700, 900, 1100, 1300
Number of Neurons for Hidden Layer 2	200, 400, 600, 800, 1000
Number of Neurons for Hidden Layer 3	100, 300, 500, 700, 900
Number of Training Epochs	500, 1000, 1500, 2000, 2500
Optimizer/Training Function	SGDM/ADAM
Initial Learning Rate	0.01
Minibatch Size	128

The mean squared error (MSE) between the actual and predicted values for each output node in relation to network training was used to measure the performance of the three neural networks. It is expressed mathematically as:

$$MSE = \frac{1}{n}\sum_{i=1}^{n}(Y_i - \hat{Y}_i) \quad (8)$$

where n is the data points number, Y_i is the actual values, and $\hat{Y}_i$ is the predicted values.

3. RESULTS AND DISCUSSION

A. Relationship of the Electrical Antenna Parameters

To ascertain the degree of relationship between the transmitter antenna operating frequency, DC input voltage, and the resulting antenna current, a Pearson correlation analysis with a 95% confidence level was carried out. In the Minitab platform, two parallel coordinate charts were created to clarify the non-linear relationships of the relevant antenna electrical characteristics (Fig. 5). The peak current and peak voltage ratings have an extremely positive correlation ($R^2 = 1$) and the antenna transmitter DC input voltage (V_{DC}) has a very strong positive correlation with the output current ($R^2 = 0.956$) which suggests that V_{DC} is a highly significant input parameter that could potentially alter the receiver voltage readings, especially with composite air and biomaterials as dielectric. On the other hand, the operating frequency of the transmitter has weak negative ($R^2 = -0.134$) and weak positive ($R^2 = 0.129$) impacts on V_{DC} and output current which confirmed that it is only responsible for the degree of resolution in the receiver side, however, it should be properly calibrated to assure capacitive resistivity operation.

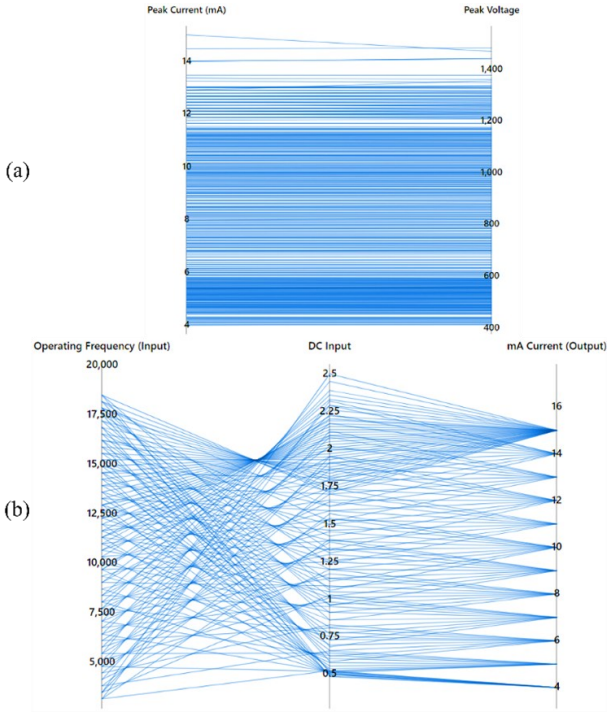

Figure 5. Parallel coordinate plots (a) between peak current and voltage ratings, and (b) among operating frequency, DC input voltage, and output current of the transmitter antenna.

B. Simulations of Recurrent Neural Network, Long Short-Term Memory, and Gate Recurrent Unit Models

The simulated current prediction models in MATLAB Software using ERNN, LSTM, and GRU are shown in Table 3. In this paper, 25 configurations of ERNN current prediction models have been trained. To train the different model combinations, The 139 patterns input-output dataset was separated into three distinct sets at random: a training data set, which makes up 56% of the data, a

validation data set, which makes up 24% of the data, and a test data set, which makes up 20% of the data. The input data used for current prediction is the measured DC input voltage of the transmitter circuit and set operating frequency ranging from 3.5 KHz to 18.5 KHz and the output data is the measured current from the measuring circuit. The training target error performance was set to $1e^{8}$. It can be observed that the trained model with hidden neuron combination of 500-200-100 and some of the trained configurations have a rapid elapsed time of less than 100 seconds due to the vanishing or exploding gradient descent encountered during training by which it is evident that one of the drawbacks of RNN is that when the network is unfolded for an excessive number of time steps or when it is processing the lengthy sequential data used in this study, the gradient of some of the weights tends to become overly small or big [30]. Since the gradient changes the weight, if the weight is set too low, the gradient will disappear, and the hidden layer next to the input layer will stop learning. On the other hand, a weight that is too large will cause the gradient to suddenly increase. RNN lacks long-term memory, so it is sensitive to time steps and will be impacted by short-term memory [28]. Moreover, six out of the 25 trained ERNN models have almost met the performance criterion of 1×10^{8}. For the current prediction ERNN model, the combination of 900-600-500 hidden neuron network models with training epochs of 2,500 has the lowest MSE during training.

Another 25 configured networks of LSTM models have been trained also for the current prediction. The simulated current prediction models using LSTM are presented (Table 3). For the input-output dataset, the 139 rows of sequential data for current prediction are divided into three: 80% for the training data, 10% as validation data, and the remaining 10% as testing data. The 'SGDM' optimizer performed well as the training function for the current prediction dataset because it aids in accelerating gradient vectors in the right directions leading to faster converging for short sequential data. From the perspective of the training time, the average running time of the LSTM model for the current prediction is 444.48 seconds. Although there are networks with less than 100 seconds of elapsed time, the LSTM models have solved the issue of vanishing or exploding gradient descent [28]. All the configured networks completed the learning process. Thus, the combination of 900-600-500 hidden neurons with 2500 training epochs achieved the lowest training MSE for the LSTM network.

The GRU models for current prediction are comprised also of 25 different networks presented in Table 3. Similar to LSTM, the input-output dataset included 139 rows of sequential data that were split into 80% training data, 10% data for validation, and the other 10% of data for testing. Since GRU is also proven to address concerns with exploding or vanishing gradient descent. All network models were learned with an average running time of 763.56 seconds. This shows that the GRU models have a slower average training time than the LSTM because the simulated networks are comprised of a complex and larger number of parameters. Hence, the 500-200-100 hidden neuron network with 1500 training epochs attained the lowest training MSE since GRU is more accurate and faster with less training parameters and a smaller dataset. Additionally, taking into account the model principle, GRU can disremember and pick memories with just one gate, while considering the fact that there are less neurons in a 500-200-100 hidden neuron network with shorter training epochs makes it accomplish the task with greater efficiency and precision than the other configurations. [28].

TABLE III. SIMULATED CURRENT PREDICTION MODELS USING ERNN, LSTM, AND GRU

Hidden Layer 1	Hidden Layer 2	Hidden Layer 3	Epochs	ERNN		LSTM		GRU	
				Training MSE	Elapsed Time (s)	Training MSE	Elapsed Time (s)	Training MSE	Elapsed Time (s)
500	200	100	500	4.41×10^{-4}	23	1.910	55	0.861	73
500	200	100	1000	1.39×10^{-7}	51	0.897	107	0.877	135
500	200	100	1500	1.28×10^{-5}	74	0.933	162	0.795	203
500	200	100	2000	4.21×10^{-5}	97	0.985	156	0.990	278
500	200	100	2500	9.90×10^{-8}	49	0.847	222	0.938	338
700	400	300	500	2.83×10^{-5}	57	1.030	107	0.892	187
700	400	300	1000	1.19×10^{-5}	114	1.020	227	0.942	312
700	400	300	1500	3.32×10^{-6}	166	0.906	224	0.796	429
700	400	300	2000	9.98×10^{-8}	194	1.030	334	0.870	597
700	400	300	2500	3.13×10^{-6}	274	0.988	384	0.798	644s
900	600	500	500	2.52×10^{-5}	107	0.981	136	0.932	228
900	600	500	1000	2.43×10^{-6}	219	0.875	181	0.898	471
900	600	500	1500	6.08×10^{-5}	312	1.080	415	0.807	631
900	600	500	2000	9.98×10^{-8}	326	0.949	537	0.933	782
900	600	500	2500	9.82×10^{-9}	354	0.845	592	0.978	1130
1100	800	700	500	6.63×10^{-2}	178	1.060	179	0.861	362
1100	800	700	1000	1.18×10^{-4}	347	1.210	200	0.949	694
1100	800	700	1500	6.04×10^{-6}	532	0.959	513	1.030	1066

1100	800	700	2000	1.80×10^{-4}	725	1.030	717	0.881	1414
1100	800	700	2500	6.13×10^{-7}	873	0.966	905	0.834	1825
1300	1000	900	500	9.03×10^{-5}	259	0.883	270	0.989	496
1300	1000	900	1000	5.31×10^{-5}	561	1.020	598	0.849	1026
1300	1000	900	1500	9.95×10^{-8}	581	0.895	870	0.868	1512
1300	1000	900	2000	6.38×10^{-4}	1047	0.860	1191	0.961	1850
1300	1000	900	2500	9.99×10^{-8}	998	0.917	1830	7.710	2424

On the other hand, the simulated voltage prediction models using ERNN, LSTM, and GRU are presented in Table 4. There are also 25 configured networks for each of the ERNN, LSTM, and GRU. In order to forecast the voltage using ERNN, 419 series of measured current from the transmitter circuit's output are used as training data, and the matching 419 series of measured voltage is utilized as the output dataset. These 419 datasets were divided into 56% for training, 24% for validation, and 20% for testing. Similar to the current ERNN prediction models, the training target error performance was set to 1×10^{8} and all the ERNN combinations of 500-200-100 hidden neurons and other trained configurations also experienced a rapid training elapsed time because of the vanishing gradient descent wherein to calculate the gradients with respect to the features in the hidden layers of the preceding time step should need an extensive amount of computation [30]. However, the ERNN combination of 1300-1000-900 hidden neurons with 2000 training epochs met the lowest training MSE for this network.

Furthermore, the simulated voltage prediction models using LSTM are given in Table 4. In the following networks, the same as ERNN, the 419 input-output datasets were also applied for the training, validation, and testing. These 419 rows are divided into 80% training data, 10% validation data, and 10% testing data. The average running time of the training period for voltage prediction using LSTM is 775.6 seconds. Also, the chosen 'ADAM' optimizer for voltage prediction worked well as the training function since it is appropriate for the optimization of larger dataset [31]. The problem with vanishing or exploding gradient descent of RNN voltage prediction models was also addressed by the LSTM voltage prediction models. Therefore, the 900-600-500 hidden neuron combination of 2500 training epochs attained the lowest possible training MSE.

Lastly, the simulated GRU voltage prediction models are shown in Table 4. The 419 input-output datasets were also applied for the training, validation, and testing. These 419 rows are divided into 80% training data, 10% validation data, and 10% testing data. The average running time of the training period for voltage prediction using GRU is 1189.09 seconds which is slower than the LSTM, but the best GRU network is the same results as the LSTM current prediction model which is the 500-200-100 hidden neuron combination of 1500 training epochs.

TABLE IV. SIMULATED VOLTAGE PREDICTION MODELS USING ERNN, LSTM, AND GRU

Hidden Layer 1	Hidden Layer 2	Hidden Layer 3	Epochs	ERNN		LSTM		LSTM	
				Training MSE	Elapsed Time (s)	Training MSE	Elapsed Time (s)	Training MSE	Elapsed Time (s)
500	200	100	500	8.23×10^{4}	4	5.69×10^{4}	91	1.02×10^{5}	134
500	200	100	1000	7.84×10^{4}	5	335	197	8.34×10^{4}	165
500	200	100	1500	7.59×10^{4}	4	163	289	8.12×10^{4}	206
500	200	100	2000	8.37×10^{4}	4	112	290	8.06×10^{4}	327
500	200	100	2500	7.55×10^{4}	4	112	376	2.12×10^{3}	407
700	400	300	500	3.230	85	182	139	7.93×10^{4}	198
700	400	300	1000	2.210	168	283	317	7.98×10^{4}	372
700	400	300	1500	1.410	256	98	473	7.99×10^{4}	557
700	400	300	2000	1.460	332	21	641	8.89×10^{4}	670
700	400	300	2500	1.940	471	31	744	8.37×10^{4}	944
900	600	500	500	2.890	177	244	234	8.02×10^{4}	320
900	600	500	1000	5.770	330	51	467	8.28×10^{4}	655
900	600	500	1500	1.550	569	27	623	8.74×10^{4}	984
900	600	500	2000	1.730	12	27	1017	8.32×10^{4}	1252
900	600	500	2500	1.190	898	16	1175	8.03×10^{4}	1739
1100	800	700	500	1.720	272	89	391	8.47×10^{4}	535
1100	800	700	1000	6.900	600	53	698	7.97×10^{4}	1168
1100	800	700	1500	0.523	889	54	1050	8.24×10^{4}	1788
1100	800	700	2000	0.834	1243	23	1278	8.24×10^{4}	2219

1100	800	700	2500	1.160	47	24	1802	8.25×10^4	2700
1300	1000	900	500	1.210	380	153	512	8.19×10^4	830
1300	1000	900	1000	0.717	808	36	971	8.34×10^4	1683
1300	1000	900	1500	0.909	63	134	1458	1.10×10^5	2319
1300	1000	900	2000	0.465	552	33	1852	8.14×10^4	3346
1300	1000	900	2500	0.915	1053	31	2305	8.09×10^4	4209

C. Evaluation of Recurrent Neural Network, Long Short-Term Memory, and GRU Model Performance

The best network models for each of the simulated ERNN, LSTM, and GRU for current and voltage prediction were consolidated in Table 5 and Table 6, respectively. After training the different networks, the selected best models were validated and tested. For the prediction of current, it can be seen from the results (Table 5) that the ERNN of 900-600-500 hidden neuron combination of 2500 training epochs outperformed the LSTM and GRU models with the lowest training MSE of 9.82×10^{-9} and a validation MSE of 1.26×10^{-8} which is lower than the test MSE of 0.587. Therefore, this configuration is selected as the best-trained model in predicting the current for the current measuring circuit of the transmitter antenna applied in underground imaging. This also shows that the ERNN provides better accuracy than the two other models due to the training hyperparameters and length of data samples.

Same with predicting the voltage, the best-simulated models for ERNN, LSTM, and GRU are shown in Table 6. From that, it has been proven that the ERNN has also bested the LSTM and GRU results. The ERNN model of 1300-1000-900 hidden neuron combination with 2000 training epochs has the lowest training MSE of 0.465, validation MSE of 0.659, and test MSE of 0.751, thus, it is selected as the best-trained model for the application of this study in predicting the voltage for measuring circuit of transmitter antenna used in underground imaging.

TABLE V. BEST MODELS FROM SIMULATED ERNN, LSTM, AND GRU NETWORKS FOR THE CURRENT PREDICTION

Model	Hidden Layer 1	Hidden Layer 2	Hidden Layer 3	Epoch	Train MSE	Validation MSE	Test MSE
ERNN	900	600	500	2500	9.82×10^{-9}	1.26×10^{-8}	0.587
LSTM	900	600	500	2500	0.845	1.06	1.51
GRU	500	200	100	1500	0.795	1.42	1.42

TABLE VI. BEST MODELS FROM SIMULATED ERNN, LSTM, AND GRU NETWORKS FOR VOLTAGE PREDICTION

Model	Hidden Layer 1	Hidden Layer 2	Hidden Layer 3	Epoch	Train MSE	Validation MSE	Test MSE
ERNN	1300	1000	900	2000	0.465	0.659	0.751
LSTM	900	600	500	2500	1.60	1.36	1.49
GRU	500	200	100	1500	2120	1690	2860

To compare the actual current from the transmitter antenna and the predicted current generated by the selected best-trained ERNN model (900-600-500 hidden neuron network of 2500 training epochs), the results are plotted in Fig. 6 as well as in Fig. 7 for the comparison of actual output peak voltage from the transmitter and predicted voltages produced by the chosen optimum trained ERNN model (1300-1000-900 hidden neuron network of 2000 training epochs). It shows that the selected ERNN models have the minimum MSE and better accuracy closer to the actual value of current and voltage signals which is essential compared to manual computations of output parameters through Ohm's Law and it is proven that RNN works effectively as presented in [16, 18] by its ability to estimate reference voltage for monitoring purposes without actually performing any measurements and in predicting electrical parameters. Compared with LSTM and GRU, the ERNN model has the ultimate advantages of fast training speed and lower predictive error in this application. The parameters that are selected and the overall amount of data may have an impact on the outcomes since RNN often works better on large datasets and with complex training hyperparameters, as prior research publications have demonstrated, and because its structure comprises feedback connections/weights that induce its memory attribute [32]. This also implies that the selected model can be implemented on the Arduino-based current measuring circuit, however, the implementation of the ERNN model has a significant impact on the computational cost given that it is a huge network that needs higher computational processing. With that, the

MATLAB Software was also not able to convert the ERNN code into its corresponding MEX function and Arduino language for execution purposes. For future studies, the researchers would like to consider exploring other deep learning approaches and changing the microcontroller with a better hardware interface, high resolution, and more powerful processing capabilities.

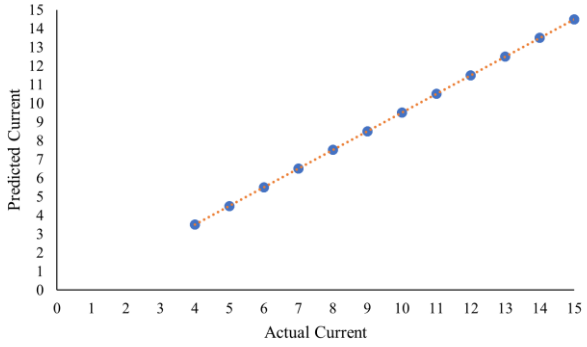

Figure 6. The plot of the actual current from the transmitter antenna circuit versus the predicted current by the configured 900-600-500 hidden neuron network of 2500 training epoch-ERNN network.

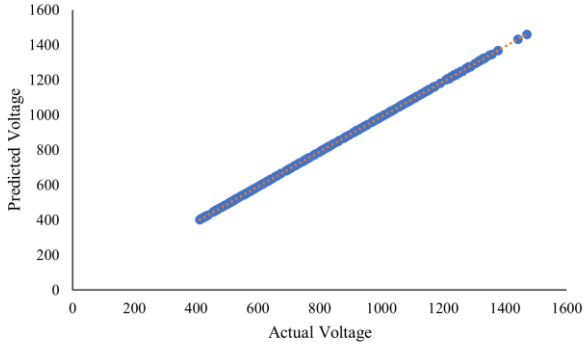

Figure 7. The plot of the actual voltage from the transmitter antenna circuit versus the predicted voltage by the configured 1300-1000-900 hidden neuron network of 2000 training epoch-ERNN network.

4. CONCLUSION

A digital meter with improved accuracy of electrical parameter readings for a single-pair antenna system of underground imaging device is developed in this study. Different neural network models are explored to predict the output current and peak voltage of the transmitter circuit designed in Proteus Software. These three neural network models are Elman recurrent neural network (ERNN), long short-term memory (LSTM), and gated recurrent unit (GRU) which are designed and simulated in MATLAB software. For the current prediction, the dataset is composed of 139 rows. The input data used are the measured DC input voltage from the measuring circuit and the operating frequency of the transmitter antenna ranging from 3.5 KHz to 18.5 KHz while the output datasets are the measured transmitter output current. On the other hand, in forecasting the output peak voltage of the transmitter system, the input and output dataset is composed of 419 rows of relationships of the transmitter peak currents and voltages ranging from 4 mA to 15 mA and 411 V_{pk} to 1485 V_{pk}, respectively. There are 25 simulated configurations designed for each of the ERNN, LSTM, and GRU networks with different combinations of hidden neurons in three hidden layers and various training epochs. Based on the lowest MSE, the performance of the prediction models was evaluated. The results show that the ERNN models both for current and voltage prediction provide the optimum accuracy with the lowest MSE. The ERNN model with a 900-600-500 hidden neuron network of 2500 training epochs outperformed the LSTM and GRU models with the lowest training MSE of 9.82×10^{-9} and a validation MSE of 1.26×10^{-8} which is lower than the test MSE of 0.587 in the prediction of output current. Additionally, the ERNN has also bested the LSTM and GRU results in predicting the output peak voltage of the transmitter antenna. The configured 1300-1000-900 hidden neuron network ERNN model with 2000 training epochs has the lowest training MSE of 0.465, validation MSE of 0.659, and test MSE of 0.751. The chosen best-trained models are deemed to be acceptable and offered a more precise output reading of current and voltage, avoiding the use of a separate, large, and multiple connection measuring device. Additionally, this enables simultaneous data acquisition through a single connection from the single-pair antenna system's transmitter for subsurface imaging. The next stage for this study is the actual implementation of the selected best models for the microcontroller used. However, it is also advisable to increase the optimization for the forecasts in real implementation by exploring other deep learning approaches and microcontrollers other than Arduino with higher power computational capabilities.

ACKNOWLEDGMENT

The authors would like to thank the Department of Science and Technology - Philippine Council for Industry, Energy and Emerging Technology Research and Development (DOST-PCIEERD) and the Intelligent Systems Laboratory of the De La Salle University for all the granted support.

References

[1] World Data Info., Population growth in the Philippines. https://www.worlddata.info/asia/philippines/populationgrowth.php, Accessed 2022-10-13.

[2] H. J. Seong and D.M. Abraham, "A decision tool for the selection of imaging technologies to detect underground infrastructure," *Tunnelling and Underground Space Technology*, vol. 19, pp.175–191, 2004, doi: https://doi.org/10.1016/j.tust.2003.09.001.

[3] A. G. Janairo, J. J. Baun, R. Concepcion, R. Relano, K. Francisco, M. L. Enriquez, A. Bandala, R. R. Vicerra, M. Alipio and E. Dadios, "Optimization of subsurface imaging antenna capacitance through geometry modeling using archimedes, lichtenberg and henry gas solubility metaheuristics," *2022 IEEE International IOT, Electronics and Mechatronics Conference (IEMTRONICS)*, pp. 1-8, 2022, doi: https://doi.org/10.1109/IEMTRONICS55184.2022.9795789.

[4] K. Francisco, R. Relano, M. L. Enriquez, R. Concepcion, J. J. Baun, A. G. Janairo, R. R. Vicerra, A. Bandala, E. Dadios and J. Dungca, "Systematic analysis and proposed AI-based technique for attenuating inductive and capacitive parasitics in low and very low frequency antennas," *IEEE International IOT, Electronics and Mechatronics Conference*, 2022, doi: https://doi.org/10.1109/IEMTRONICS55184.2022.9795784.

[5] K. Francisco, R. Concepcion, R. Relano, M. L. Enriquez, J. J. Baun, A. P. Mayol, J. Española, R. R. Vicerra, A. Bandala, E. Dadios, A. Ubando and H. Co, "Analytical hierarchical process-based material selection for trailer body frame of an underground imaging system," *2021 IEEE 13th International Conference on Humanoid, Nanotechnology, Information Technology, Communication and Control, Environment, and Management (HNICEM)*, pp. 1-6, 2021, doi: https://doi.org/10.1109/HNICEM54116.2021.9732048.

[6] L. Lo Monte, D. Erricolo, F. Soldovieri and M. C. Wicks, "Underground imaging of irregular terrains using RF Tomography," *2009 3rd IEEE International Workshop on Computational Advances in Multi-Sensor Adaptive Processing (CAMSAP)*, pp. 229-232, 2009, doi: https://doi.org/10.1109/CAMSAP.2009.5413292.

[7] O. Kuras, D. Beamish, P. I. Meldrum and R. D. Ogilvy, "Fundamentals of the capacitive resistivity technique," *Geophysics*, vol. 71, no. 3, 2006, doi: https://doi.org/10.1190/1.2194892.

[8] R. D. Ogilvy, P. I. Meldrum, O. Kuras and D. Beamish, "Systems and methods for resistivity measurement," 2009, doi: https://nora.nerc.ac.uk/id/eprint/20124.

[9] M. N. A. Karim, M. F. A. Malek, M. F. Jamlos, L. Y. Seng and N. Saudin, "Design of Ground Penetrating Radar antenna for buried object detection," *2013 IEEE International RF and Microwave Conference (RFM)*, pp. 253-257, 2013, doi: https://doi.org/10.1109/RFM.2013.6757260.

[10] M. Alesheikh, R. Feghhi, F. M. Sabzevari, A. Karimov, M. Hossain and K. Rambabu, "Design of a high-power Gaussian pulse transmitter for sensing and imaging of buried objects," *in IEEE Sensors Journal*, vol. 22, no. 1, pp. 279-287, 2022, doi: https://doi.org/10.1109/JSEN.2021.3127136.

[11] M. Bimpas, A. Amditis, and N.K. Uzunoglu, "Design and implementation of an integrated high resolution imaging ground penetrating radar for water pipeline rehabilitation," *Water Resources Management,* vol. 25, pp.1239–1250, 2010, doi: https://doi-org.dlsu.idm.oclc.org/10.1007/s11269-010-9631-y.

[12] K. Tingting, L. Yan, Z. Lei and H. Yan, "Development of multi-channel automatic digital multimeter calibration device," *14th IEEE International Conference on Electronic Measurement & Instruments*, 2019, doi: https://doi.org/10.1109/ICEMI46757.2019.9101487.

[13] P. Petrovic, "New digital multimeter for accurate measurement of synchronously sampled AC signals," *IEEE Transactions On Instrumentation and Measurement*, vol. 53, no. 3, 2004, doi: https://doi.org/10.1109/TIM.2004.827313.

[14] F. Sha, M. Liu, and X. Chen, "The design of digital multimeter automatic calibration system and application of PID algorithm," *IEEE 8th Joint International Information Technology and Artificial Intelligence Conference*, 2019, doi: https://doi.org/10.1109/ITAIC.2019.8785866.

[15] N. Pătrăşcoiu and I. C. Barbu, "Data-logger built using a digital multimeter and virtual instrumentation," *Proceedings of the 14th International Carpathian Control Conference (ICCC)*, pp. 288-291. 2013, doi: https://doi.org/10.1109/CarpathianCC.2013.6560555.

[16] I. Nantovska, D. Fefer and A. Jeglic, "Predictive models for voltage reference elements monitoring," *IEEE Instrumentation and Measurement Technology Conference*, 2001, doi: https://doi.org/10.1109/IMTC.2001.929473.

[17] M. L. Enriquez, R. Concepcion, R. Relano, K. Francisco, A.P. Mayol, J. Española, R. R. Vicerra, A. Bandala, H. Co, and E. Dadios, "Prediction of weld current using deep transfer image networks based on weld signatures for quality control," *IEEE 13th International Conference on Humanoid, Nanotechnology, Information Technology, Communication and Control, Environment, and Management*, 2021, doi: https://doi.org/10.1109/HNICEM54116.2021.9731979.

[18] A. Rahman, V. Srikumar and A. D. Smith, "Predicting electricity consumption for commercial and residential buildings using deep recurrent neural networks", *Applied Energy*, vol. 212, pp. 372–385, 2018, doi: https://doi.org/10.1016/j.apenergy.2017.12.051.

[19] R. DiPietro and G. D. Hager, "Chapter 1- Deep learning: RNNs and LSTM, Handbook of medical image computing and computer assisted intervention," pp. 503-519, 2020, doi: https://doi.org/10.1016/B978-0-12-816176-0.00026-0.

[20] T. K. Gupta, K. Raza, "Optimization of ANN Architecture: A review on nature-inspired techniques," in: N. Dey, S. Borra, A.S. Ashour, F. Shi (Eds.), Machine Learning in Bio-Signal Analysis and Diagnostic Imaging, Elsevier, 2019, pp. 159-182. https://doi.org/10.1016/B978-0-12-816086-2.00007-2.

[21] X. Zhang, Y. Wang, Y. Zheng, R. Ding, Y. Chen, Y. Wang, X. Cheng and S. Yue, "Reactive load prediction based on a Long Short-Term Memory Neural Network," *in IEEE Access*, vol. 8, pp. 90969-90977, 2020, doi: https://doi.org/10.1109/ACCESS.2020.2991739.

[22] H. Wang, X. Huang, S. Gao, Z. Yang, T. Gao, Q. Zhao and H. Ding, "Electric vehicle charging load clustering and load forecasting based on long short term memory neural network," *2022 IEEE 5th International Electrical and Energy Conference (CIEEC)*, pp. 3196-3200, 2022, doi: https://doi.org/10.1109/CIEEC54735.2022.9846570.

[23] M. Barati, "Faster than real-time prediction of disruptions in power grids using PMU: Gated Recurrent Unit approach," *2019 IEEE Power & Energy Society Innovative Smart Grid Technologies Conference (ISGT)*, pp. 1-5, 2019, https://doi.org/10.1109/ISGT.2019.8791625.

[24] Q. Niu and L. Wang, "Real-time inverter semiconductor die temperature estimation using inverter operating condition-based Gate Recurrent Unit," *2018 9th IEEE International Symposium on Power Electronics for Distributed Generation Systems (PEDG)*, pp. 1-6, 2018, doi: https://doi.org/10.1109/PEDG.2018.8447642.

[25] O. Kuras, "The capacitive resistivity technique for electrical imaging of the shallow subsurface," University of Nottingham, 2002, doi: http://eprints.nottingham.ac.uk/10171/1/PhD_Kuras_Oliver_2002.pdf.

[26] R. Barika and O. Faust, "A review of automated sleep stage scoring," in: C. Cirelli, S. Nallu, S. Nishino, M.E. Dyken, J. Ong,

J. Zeitzer, E. Olson, B. Selim, J. Winkelman, T. Hoban, S. Leibowitz, M. Wise; C. Depner (Eds.), Encyclopedia of Sleep and Circadian Rhythms, second ed., Elsevier, 2023.

[27] Z. Hamad and I. Abdulrahman, "Deep learning-based load forecasting considering data reshaping using MATLAB\Simulink," *International Journal of Energy and Environmental Engineering*, vol. 13, no. 3, pp. 853–869, 2022, doi: https://doi.org/10.1007/s40095-022-00480-x.

[28] S. Yang, X. Yu and Y. Zhou, "LSTM and GRU neural network performance comparison study: Taking yelp review dataset as an example," *2020 International Workshop on Electronic Communication and Artificial Intelligence (IWECAI)*, pp. 98-101, 2020, doi: https://doi.org/10.1109/IWECAI50956.2020.00027.

[29] X. H. Le, H. V. Ho, G. Lee, S. Jung, "Application of Long Short-Term Memory (LSTM) neural network for flood forecasting," Water (Switzerland), vol. 11, p. 387, 2019, doi: https://doi.org/10.3390/w11071387.

[30] S. Kumar, L. Hussain, S. Banarjee and M. Reza, "Energy load forecasting using deep learning approach-LSTM and GRU in spark cluster," *2018 Fifth International Conference on Emerging Applications of Information Technology (EAIT)*, pp. 1-4, 2018, doi: https://doi.org/10.1109/EAIT.2018.8470406.

[31] D. P. Kingma and J. Ba, "Adam: A method for stochastic optimization," *in: 3rd International Conference on Learning Representations*, 2015, doi: https://doi.org/10.48550/arXiv.1412.6980.

[32] T. Gupta and S. N. Sachdeva, "Recurrent neural network-based prediction of compressive and flexural strength of steel slag mixed concrete," *Neural Comput & Applic*, vol. 33, pp. 6951–6963, 2021, doi: https://doi.org/10.1007/s00521-020-05470-w.

Author 1 Ms. Jonah Jahara Baun is a researcher associated with De La Salle University. In 2020, she received her B.Sc degree in Electronics and Communications Engineering from the Polytechnic University of the Philippines-Manila. Following her academic achievements, she joined De La Salle University in 2022 for her M.Sc degree of the same engineering field. Her main work revolves around the development of Capacitive Resistivity Underground Imaging System Equipment. Ms. Baun is a member of the Institute of Electrical and Electronics Engineers (IEEE) and an Associate Member at the National Research Council of the Philippines.

Author 2 Mr. Adrian Genevie Janairo is a researcher affiliated with De La Salle University. In 2020, he received his B.Sc degree in Electronics and Communications Engineering from the University of Santo Tomas. Shortly after, he joined De La Salle University in 2021 for his graduate studies. His primary focus and main work revolve around the development of Capacitive Resistivity Underground Imaging System Equipment.

Author 3 Dr. Ronnie S. Concepcion II is an outstanding young scientist and researcher associated with De La Salle University. In 2021, he completed his Ph.D. degree at De La Salle University and immediately joined the institution as an Associate Professor. His primary area of research revolves around the development of non-destructive techniques for crop phenotyping. His work focuses on employing integrated machine vision and computational intelligence to study crops at the molecular, organelle, and system levels. By utilizing these innovative approaches, Dr. Concepcion aims to contribute to sustainable and precision agriculture practices. He is a member of the Institute of Electrical and Electronics Engineers (IEEE) and holds regular membership in the National Research Council of the Philippines.

Author 4 Ms. Kate Francisco is a researcher affiliated with De La Salle University (DLSU). She holds a B.Sc degree in Manufacturing Engineering from Bulacan State University and joined De La Salle University in 2021 to further his academic and professional pursuits. For now, her focus is in the development of Capacitive Resistivity Underground Imaging System Equipment. Ms. Francisco is a member of the Institute of Electrical and Electronics Engineers (IEEE) and an Associate Member at the National Research Council of the Philippines.

Author 5 Mr. Mike Louie Enriquez is a researcher associated with De La Salle University. He received his B.Sc degree in Manufacturing Engineering from Bulacan State University in 2018 and currently taking his Master's degree at DLSU for the same engineering field. His main focus lies in the development of Capacitive Resistivity Underground Imaging System Equipment. Mr. Enriquez is a member of the Institute of Electrical and Electronics Engineers (IEEE) and an Associate Member at the National Research Council of the Philippines.

Author 6 Mr. R-Jay Relano received his B.Sc degree in Mechanical Engineering from Bulacan State University in 2010. In 2021, he joined De La Salle University for his M.Sc degree in Manufacturing Engineering, where he is currently affiliated. His main work involves being the engineer in charge of designing the mechanical component of a towed imaging system. This responsibility showcases his expertise in mechanical design and his ability to contribute to the development of advanced imaging systems.

Author 7 Dr. Edwin Sybingco distinguished academic and researcher affiliated with De La Salle University. He completed his Ph.D. degree at De La Salle University, highlighting his expertise and commitment to advancing knowledge in his field. His main area of work centers around the application of computer vision, machine learning, deep learning, robotics, and signal processing. Dr. Sybingco is a member of the Institute of Electrical and Electronics Engineers (IEEE).

Author 8 Dr. Argel Bandala is a distinguished academic and researcher associated with De La Salle University. He joined the university in 2012 and has made significant contributions to his field. In 2014, he received his Ph.D. degree from the same institution. His main focus lies in the development of a swarming algorithm for unmanned aerial vehicles (UAVs). Through his work, he explores innovative approaches to enable UAVs to operate collaboratively and autonomously in swarms. Dr. Bandala is a member of the Institute of Electrical and Electronics Engineers (IEEE).

Author 9 Dr. Ryan Rhay Vicerra is a distinguished academic and researcher affiliated with De La Salle University. In 2014, he completed his Ph.D. degree at De La Salle University, highlighting his expertise and commitment to advancing knowledge in his field. His main area of work centers around swarm intelligence for underwater swarm robot systems. He has dedicated his efforts to the development of an underwater swarm robot system, utilizing swarm intelligence techniques. Through his research, he aims to enhance the capabilities of underwater robotics and contribute to the exploration and understanding of aquatic environments. Dr. Vicerra is a member of the Institute of Electrical and Electronics Engineers (IEEE).